

# Superresolution technique beyond the diffraction limit under a structured beam via different optical nanostructures

Subhankar Roy<sup>1</sup>, Jianping Hu<sup>2</sup> and M Ummal Momeen<sup>1\*</sup>

<sup>1</sup>*Magnetic Instrumentation and Applied Optics Laboratory, Department of Physics, School of Advanced Sciences, Vellore Institute of Technology, Vellore, Tamil Nadu, 632014, India.*

<sup>2</sup>*Applied Nuclear Technology in Geosciences Key Laboratory of Sichuan Province, Chengdu University of Technology, Chengdu, People's Republic of China.*

\**ummalmomeen@gmail.com*

## **ABSTRACT:**

To overcome the limit of diffraction while achieving the superresolution technique, solid immersion lenses are the key optical elements for data storage and nanophotonics applications. Recent demonstrations have shown how different nanostructures (such as elliptical SILs) are used in diverse fields of increasing resolution in the presence of a structured Gaussian beam. By applying twisted beams such as angular momentum beams (Laguerre- Gaussian) and spatial higher-order Gaussian beams (Hermite- Gauss), we can attain a sharp (FWHM = 27 nm) near-field focal spot pattern, which is considerably better than the conventional macroscopic SIL. By numerical simulations, tolerance has been confirmed with a slight variation in beam size and geometrical modification to make the model compatible with fabrication errors. This narrow bandwidth intensity distribution can be utilized for scanning the sample with higher resolution, especially in the field of quantum technology.

## **Introduction:**

In optical microscopy, fluorescence-based light manipulation to acquire resolution in the subwavelength regime is quite challenging. Breaking the barrier of the Abney diffraction limit to attain superresolution in the subwavelength region is highly demanding for resolving nanoscale particles/specimens in optics. The diffraction limit significantly restricts the resolution between adjacent particles while scanning through a sample because of the exponential decay of evanescent waves, which carry subwavelength information in the far-field domain [1]. Near-field optical resolution can be used to analyze subwavelength structures such as tapered fibers, optical nanoantennas, and nanoscale needles through the coupling of light near the surface of a sample [2, 3]. However, the resolution limit while measuring through a conventional optical system is

approximately half the wavelength of the incident beam, which is treated as a constraint of our final resolved image [1].

Initially, the design of the super lens was potentially capable of retrieving the evanescent wave to achieve higher resolution in imaging [4]. The design of such a lens effectively converts evanescent waves into propagating waves in the near-field region, as they are engineered by a negative index material. Few optical superlenses are fabricated from silver or SiC, which works well in the infrared and ultraviolet wavelength regions [5,6]. On the other hand, silver metal substantially supports evanescent wave transport without decaying much inside the silver slab, which effectively carries information [4]. However, these optical systems suffer from few drawbacks, which substantially hinder further applications. These lenses generate heat while scanning the sample,

which in turn damage and affects the target material during optical imaging under white light illumination [7]. Therefore, building a geometry that works under all visible spectra is highly desirable [7]. Later, hyperlenses were proposed and fabricated to increase the resolution by using metamaterials, which also suffer from inevitable manufacturing limitations [8]. To overcome this, nanorange lenses (solid immersion lenses (SILs)) with dielectric materials have been developed, which undergo low loss and cross the diffraction limit barrier for subwavelength imaging. These nanorange models are able to produce better resolution than the normal macroscopic SIL [9]. Even the inclusion of high-refractive-index materials can immensely increase the resolution below 100 nm [9,10].

Nevertheless, out of several optical approaches [11, 12], SIL has been extensively studied because of its exceptional performance in improving the superresolution ranging from the micrometer size to the nanoscale regime [13]. These SILs show efficient development in terms of near-field resolution under different kinds of wave illuminations, such as plane wave, Gaussian wave, and dark field incidence, beyond the diffraction limit. Even though different structured beams can create subdiffraction focal spots, they still cannot reach resolutions below 100 nm. Recently, vector beams have drawn significant interest because of the beam polarization of propagating beams in the spatial direction. Spatially dependent polarization in the cross section of the beam profile is crucial for determining the resolution in the subwavelength domain, as it involves orbital angular momentum (OAM). This OAM encompasses a helical phase distribution to the photons in terms of information in higher dimensions. This circularly polarized beam is inherently related to the intensity distribution, which provides an annular shape during beam propagation. Some studies have been based on vortex beams but have not explored high-index lenses to improve the resolution. A Gaussian beam is a typical OAM beam associated with a quantized phase change. Several quantum optical applications, such as tight beam focusing, superresolution imaging, manipulation of micromechanical reactions and optical trapping,

are realized due to the interaction between this polarized state and material interactions. Another spatially distributed beam, such as the Hermite Gauss beam, enhances the resolution beyond the diffraction limit when it is coupled with subwavelength high-index optical nanostructures, as discussed in a later section.

In the first part of our study, we presented a systematic study in combination with a high-index material based optical structure to achieve diffraction limited near-field spot under three different structured beam illuminations (Gaussian beam, dark field and Laguerre Gaussian (LG) beam). We demonstrate a design concept supported by simulation results based on an LG beam with a diamond e-SIL structure, which provides superresolution below 100 nm.

Even though a dark field is able to cross the diffraction limit, a twisted beam (LG beam) still employs a prevailing technique to achieve our aim by generating nanoscale local electric field spots in the superresolution regime. We compared the FWHM values of the near-field intensity patterns of three different incident beams. Finally, we present a resolution even below 70 nm under LG beam illumination by our optimized model. By varying the geometry size and beam waist, we confirmed the robustness of our optimized design.

We also utilize an alternative higher-order Gaussian beam, i.e., the Hermite Gauss beam, to improve the resolution in the subwavelength region, as this also stimulates spatial components of the beam to achieve highly resolved images. Our numerical analysis confirms that our HG beam with a specified mode is able to generate a subwavelength near the electric field spot in association with a nano SIL with a higher refractive index. The use of different structured beams with nanostructures provides excellent performance in superresolution imaging at the interface between the nanostructure and air, which has a wide range of applications ranging from quantum sensing [14] to biological imaging [15].

We also made a study to modify the geometry by introducing a cone, cylinder and pyramidal shaped structures to enhance the overall system

performance by obtaining an FWHM value of 27 nm. By varying the dimensions of the geometry and the different beam waists, we tested the robustness of the proposed model. These nanostructures can be utilized as nanorange lenses with modified focal lengths and wider numerical apertures for near-field optical imaging.

## Results and discussion

Figure 1(a) depicts a schematic design of our simulation scheme. Superresolution can be achieved either by considering a high-index substrate with evanescent wave excitation or placing subwavelength nanostructures in close proximity to the scanning object. Here, we consider a high-index solid immersion lens to construct a subdiffraction focal spot at the plane surface of the lens. Coherent monochromatic incident light source illumination with different beam profiles is realized through our SIL structure to achieve superresolution in the subwavelength domain. Even though two different types of geometries (e-SIL and cone) are considered, major attention is given to SIL-based nanolens structures, which are described with structural modifications for determining resolutions below 100 nm. Indeed, this high-index material (diamond) results in low loss and a more confined beam profile inside the optical structure by improving the overall system performance in terms of resolution. A high-index

e-SIL improves the beam focus inside the lens structure because of the high contrast in the refractive index value at the air-SIL interface. To enumerate a slight shift in the focal spot due to the change in the refractive index after placing the lens structure, we consider the optimized position of the nanolens in such a way that it coincides with the focal spot of the incident Gaussian beam. Furthermore, the numerical aperture also simultaneously increased because of the curved surface of the SIL outer interface.

Special attention is given to the bottom surface of the e-SIL and the cone structure, as the field distribution is calculated at that plane to measure the resolution strength after the incident beam converges at the focal plane inside the high-index SIL structure.

This plane is kept as a reference while scanning any sample via our nanoscale structures; hence, it is commonly known as the plane of interest (POI). The near-field distribution is the basis of subwavelength imaging when we deal with structured beam illumination, and indeed, the propagation plane of each incident beam plays a significant role in orthogonally intersecting the POI at the plane surface of the optical structure.

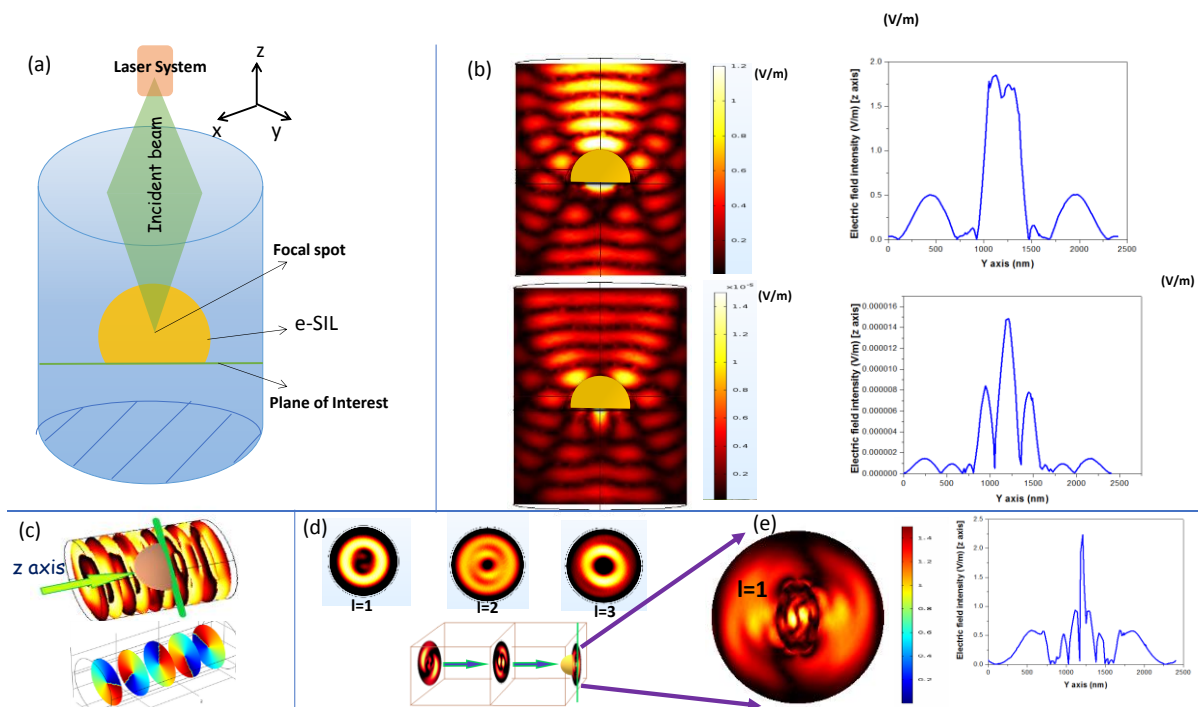


Fig. 1: Schematic diagram of the optical system for the superresolution scheme. (b) Electric field distribution while the plane Gaussian beam and dark field are incident on our diamond-based ellipsoid optical nanostructure. (c) Laguerre Gaussian beam is launched toward the z-axis from a circular aperture. (d) Different modes of the LG beam are shown, and finally, we work with the optimized mode  $l=1$ , i.e., the basic mode of the LG beam. (e) Cross-sectional view of the near-field distribution at the plane of interest after SIL is placed. The near-field distribution is achieved with an FWHM of 60 nm.

To determine the FWHM value of the intensity pattern, we focus on the near electric field distribution, which is intrinsically linked with the resolution, i.e., the smallest value of the FWHM yields the highest resolution in the lateral direction. In general, we calculate a normalized distribution of the near electric field pattern ( $|E^2|$ ) at  $x=0$  on the  $y$ -axis plane from the POI to calculate the full width at half maximum (FWHM) value. We address a numerical calculation to mimic the experimental environment by considering a cylindrical simulation area. Different incident beams with a circular aperture of 700 nm are focused on the nanoscale lens structure (made of diamond material) via the cylindrical geometry shown in Figure 1(a).

The optimized height and semi-major axes of e-SIL are considered to be 420 nm and 500 nm under the excitation wavelength ( $\lambda = 532$  nm). From our study, it is clear that the position of the incident aperture and the focal plane of the beam cause a consequential variation in the electric field distribution. Hence, the system needs stable optimization, which produces high resolution in terms of the intensity distribution even with a slight variation in the simulation parameters. Initially, the analysis begins by focusing a user-defined Gaussian beam [Figure 1(b)] inside the ellipsoid diamond solid immersion lens (e-SIL) optical structure. We define the wave function for launching a plane Gaussian beam as expressed below.

$$\psi(x, y, z, t) \sim e^{-\frac{(x^2+y^2)}{\omega^2}} A_0 e^{i(kz-\omega t)} e^{\frac{ik(x^2+y^2)}{2R(z)}}$$

where  $\psi$  is the complete wave function for the Gaussian wave distribution, which consists of a Gaussian beam profile, unidirectional beam propagation and wave-front curvature.  $A_0$  is the amplitude of the incident beam profile, and  $R(z)$  is the radius of curvature of the beam profile. The

ideal focal point is kept at  $z=0$  in the simulation coordinate system. We have ignored the negligible impact of the paraxial approximation and the shift in the focal point even after nanostructure insertion. Figure 1 shows the electric field intensity distribution at the POI when three different beams are incident on the optimized model. The highest resolution is achieved with the application of the Laguerre Gaussian (LG) beam, which is discussed in a later section. Figure 1(b) shows the normalized near-field distribution with gradual optimization in the side lobes when a user-defined Gaussian beam profile is launched into the focal plane; correspondingly, an FWHM value of 360 nm is achieved at the POI. The resolution strength is failed to reach a value beyond the diffraction limit, and the near-field distribution is accompanied by small side lobes. The contrast between the side lobes and main peak is quite large at the POI. This approach results in a wider window while scanning any sample or substrate at the POI of our proposed optical nanostructure during resolution estimation.

Therefore, further modifications in the incident beam profile are crucial for improving the resolution of our optimized model. Dark field illumination with distinctive high-contrast properties is launched via the combination of two Gaussian beams of the same size with a  $\pi$  phase difference. We assume a straightforward approach by considering two beam profiles with the same size and amplitude, with the exception of their phase, to make our simulation easier. By reshaping the above mentioned Gaussian beam profile with the same focal point, we express the dark field illumination as

$$\begin{aligned} & \psi(x, y, z, t) \\ &= A_0 \frac{\omega_0}{\omega(z)} e^{-\frac{(x^2+y^2)}{\omega(z)^2}} e^{i(kz-\omega t)} e^{\frac{ik(x^2+y^2)}{2R(z)}} e^{-i\varphi(z)} \\ &+ A_0 \frac{\omega_0}{\omega(z)} e^{-\frac{(x^2+y^2)}{\omega(z)^2}} e^{i(kz-\omega t+\pi)} e^{\frac{ik(x^2+y^2)}{2R(z)}} e^{-i\varphi(z)} \end{aligned}$$

Figure 1(b) presents a significant drop in the FWHM value (175 nm) of the near-field intensity pattern, making it quite better in terms of resolution performance accompanied by dominant side lobes. The energy density of the main peak is greater than that of the side lobes, which are treated as the dominant peak for resolution estimation. We obtained a subdiffraction-limited FWHM value that is reduced by almost  $\sim 200$  nm less than our Gaussian illumination in this attempt. Even though the resolution limit crosses below the diffraction limit near the field spot generated at the center, side lobes are still present in the intensity distribution. Next, we applied this dark field to our optimized e-SIL structure with lower-index materials, commercially available lenses, as previously described, for a comparative study. The results provided by these systems are not as competitive as those of the diamond e-SIL optical structure, which is discussed in the next section.

Considering our prime requirement, we introduce a different structured beam called Laguerre Gaussian onto our high-index diamond-based e-SIL structure as a new approach (Figure 1(c)) for the application of twisted beams. Even though a dark field can cross the diffraction limit, a twisted beam profile (LG beam) is still the prevailing technique to achieve better accuracy in terms of resolution, which can reach below 100 nm and is not the case with dark field illumination. Different techniques can be adopted to form LG beams, such as spiral phase plates and multimodal crystals. The phase component  $\exp(i\varphi)$  generates orbital angular momentum. The phase singularity in the beam axis while propagating leads to a null electric field distribution in the middle of the LG beam. This beam profile corresponds to a donut shaped or concentric ring field distribution that excites only the spatial distribution of the beam structure, which helps to obtain information in the superresolution regime (i.e., below 100 nm). This beam is focused on a curved surface of the diamond lens. The high-index lens directs the circular spatial beam profile to a converging point, which slightly moves from the original focus point. Finally, at the interface between air and lens, looking at the near-field distribution, tiny focal spots such as a photonic nanojet shape, which is in the superresolution regime, are generated.

Our key prerequisite is to implement the spiral phase front beam or vortex beam with the diamond e-SIL to converge into a subdiffraction focal spot. Generally, this beam consists of a polynomial term that defines the mode of the LG beam, i.e.,  $L_m^n$ . The radial mode number  $m$  and the angular mode number  $n$  should be specified along with the equation. We initiate an approximated Laguerre Gaussian beam in the COMSOL simulation environment, which is represented for our particular structure via the following equation:

$$E_{0,1}(r, z) = E_0 e^{i\varphi} \frac{r}{\omega(z)} \exp\left(i\left(\psi_{0,1}(z) - \psi_{0,0}(z)\right)\right) E_{0,0}(r, z)$$

We consider a basic-order LG beam for our simulation, where the angular mode number is considered to be 1 (Figure 1(d)) for LG beams of different orders. With the presence of this beam, we attempt to inspect the improvement in resolution by our model at the same POI. The highest resolution is obtained, which is  $\sim 60$  nm at its optimum position (Figure 1(e)). Even though side lobes are present, because electric field distribution is less at the POI inside those lobes, a significant difference in the resolution is not observed. The resolution efficiency increased significantly under LG beam illumination compared with Gaussian and dark field illumination, respectively.

### Geometrical tolerance of the optical structure

The variation in the resolution and near-field intensity distribution at the POI with respect to the beam waist of the applied beam and the geometry of the e-SIL structure along the  $yz$  plane should be tested to verify the robustness of the complete system. The intensity distribution corresponding to a wide range of beam waist variations ranging from 700 nm to 900 nm for the three applied beams is shown in Figure 2, while the other model parameters remain at their optimum values. We achieve a resolution efficiency of  $(\lambda/8.5)$  when the beam waist is 700 nm. The green plot shows that the variation in the FWHM value from the optimum value does not exceed  $\sim 20$  nm.

Figure 2 shows a comparative study to validate that our high-index material with LG beam incidence provides a substantial improvement in resolution compared with other commonly used lens materials, such as silica (r.i.=1.46) and

polymers (r.i.=1.6). The evolution in resolution was recorded in the presence of three different incident beams such as Gaussian, dark-field and Laguerre–Gaussian beams, in those plots.

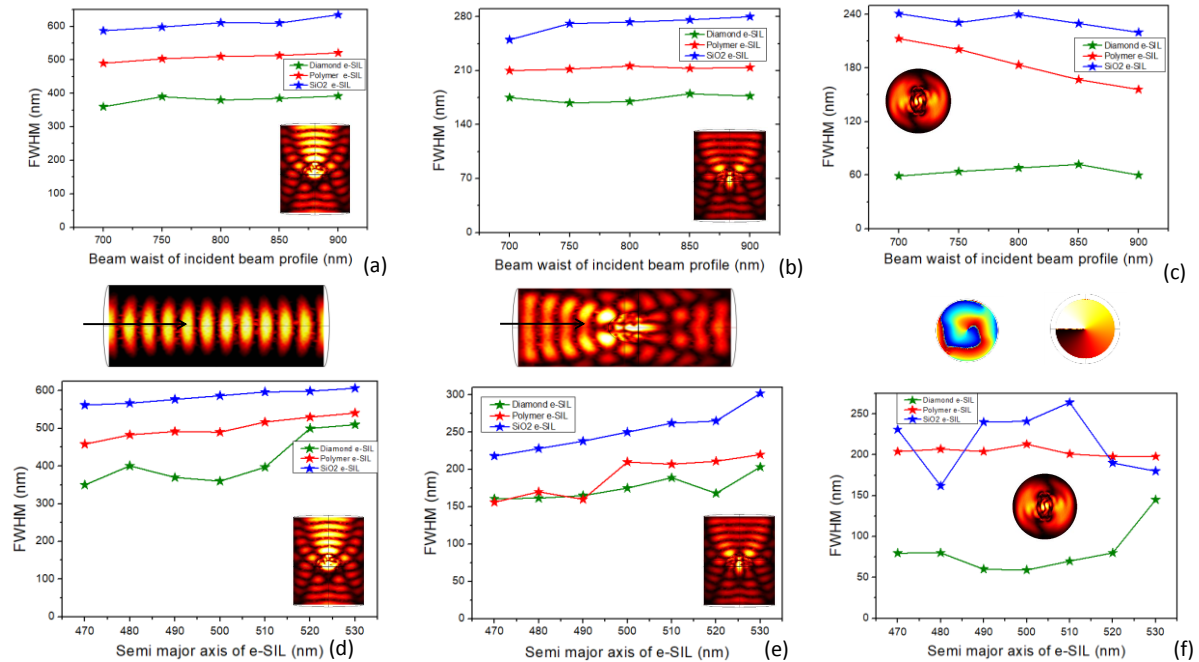


Fig. 2: Tolerance check when three different beams are launched, i.e. Gaussian, dark field and LG beams, on three different lens materials. (a) and (d) Resolution deflection is shown while the beam waist and semimajor axis are changed for the plane Gaussian beam. (b) and (e) Same analysis under dark field and (c) and (f) LG beam illumination.

Figure 2(a) shows a detailed comparison of three different lens materials (silica, polymer and diamond) under Gaussian beam illumination with respect to the beam waist of the incident beam. Moving toward a higher beam waist indicates a minimal deviation of  $\pm 8$  nm in the FWHM value, which is negligible and cannot influence the main lobe sensitively. The resolution efficiency in terms of FWHM values shows poor resolving power under this Gaussian beam. However, this opens a large window, facilitating a wider view of the object while scanning, which is undesirable for any subwavelength imaging technique. Nevertheless, the diamond-based lens produces higher resolution than the other two lens materials. Later, we checked while varying the semimajor axis of the e-SIL and thus also provide poor resolution efficiency, as shown in Figure 2(d). The diamond lens has better resolution when the semimajor axis value is near 500 nm. The fluctuation is slightly

greater for the diamond lens under Gaussian illumination than for the other two lenses.

Nevertheless, deflection in terms of resolution strength is further calculated under dark field incidence w.r.t. different beam waists for three different lens materials. The minimal deflection in the FWHM measurement ( $\sim \pm 3$  nm) is observed for the diamond and polymer lens structures (Figure 2(b)); however, for SiO<sub>2</sub>, it shows  $\pm 12$  nm variation due to the lower index material. Here, the converging beam pattern inside the structure significantly changes with increasing beam waist. The same tolerance is applied w.r.t. the geometry of the e-SIL structure (Figure 2(e)), which results in a  $\pm 20$  nm deviation in the resolution efficiency for all three different lens materials. From this analysis, we can observe that the side lobe intensities are more dominant than Gaussian illumination because more energy is concentrated at the POI. The diamond lens also shows better

stable performance than the other two lens materials. The fluctuation in the resolution performance over a wide range of semimajor axes is slightly greater because of the structural modification in the nanolens, which has a significant effect on beam convergence. Even though the resolution efficiency exceeds the diffraction limit, we still cannot achieve resolution via this dark-field illumination near the superresolution regime, i.e., below 100 nm.

Furthermore, we calculate the robustness of the optimum structure under LG beam illumination w.r.t. same parametric sweep. This numerical study confirmed that an LG beam can yield a highly resolved image when it is incident on a diamond e-SIL at our optimized beam waist. The dominance in the side lobes proves that more energy is concentrated on those lobes at higher applied beam waists, as shown in Figure 3(c). This provides a negligible deflection in the resolution efficiency, i.e.,  $\pm 8$  nm, toward a higher waist size. In the case of polymers and SiO<sub>2</sub> lenses, LG beams could not cross the barrier of the superresolution limit, which is a drawback for those materials. The poor performance in terms of the resolution of these available lens materials makes our diamond e-SIL favorable for subwavelength imaging. A shift in the focal point near the e-SIL-air interface, i.e., close to the plane of interest, can sometimes intensify the near-field spot and resolution, confirming the stability of the performance in the field of nanoimaging.

Importantly, the comparison between the FWHM when the geometry of the e-SIL is modified along the y-axis is important. Continuing the above discussion, we inspect the variation in the intensity profile while the semimajor axis is altered along the YZ axis for all these lenses. Figure 2(f) shows the deflection in the near-field spot under Laguerre Gaussian beam illumination, while the semimajor axes of e-SIL vary within a broad range of  $\pm 30$  nm from the optimized model. In the case of other materials, this geometry tolerance results in large deviations/random fluctuations in the resolution performance even though the resolving power is poor compared with that of other incident beams in this case.

To determine the robustness of the resolution efficiency, we achieve stable variation under a plane Gaussian beam. Nevertheless, owing to the higher value ( $\sim 500$  nm, i.e., much closer to the incident wavelength) of the FWHM, the resolution efficiency decreases drastically. Rather, in dark-field illumination, crossing the optimized limit elucidates that the side lobe intensities are slightly enhanced by decreasing the resolving power. Figure 2(f) demonstrates truncating the lateral radius below 500 nm of e-SIL causes a reduction in resolution. In the case of LG beam application, the FWHM values decreased below 100 nm in the superresolution regime at the optimized position. This optimization in the geometry modification helps to reach a value of  $(\lambda/8.8)$ , i.e., the smallest resolution efficiency that one could expect in this scheme, but the sharpness of the resolution also decreases.

#### Hermite Gaussian beam illumination:

Here we introduce another higher-order Gaussian beam profile known as the Hermite Gauss beam. This beam is composed of a solution of the Paraxial Helmholtz equation, and it evolves with different modes on the basis of the polynomial functions. We have fed the general Hermite- Gaussian beam profile in our incident aperture, and the near electric field distribution is demonstrated in Figure 3(a). The beam is expressed as

$$E_{m,n} = E_0 \frac{\omega_0}{\omega(z)} e^{-\frac{(x^2+y^2)}{\omega(z)^2}} e^{i(kz)} e^{\frac{ik(x^2+y^2)}{2R(z)}} e^{-i(1+n+m)\varphi(z)} H_m\left(\frac{\sqrt{2}x}{\omega(z)}\right) H_n\left(\frac{\sqrt{2}y}{\omega(z)}\right)$$

where  $H_m$  and  $H_n$  are the Hermite polynomials, which have different modes depending on the m and n values. The generation of different modes, such as (00) (10), (01), (11), (12) and (02), is illustrated in Figure 3(b), which converges after falling on a high-index e-SIL structure. Owing to different field distributions, the near-field focal spot yields a sharp FWHM in the superresolution regime at the POI in the YZ plane. Our numerical analysis confirmed that it is possible to produce more than two highly resolved peaks at the POI in

higher-order modes with different optimized parameters. Different modes in the beam profile signify the spatial distribution of the beam, such as

the LG beam, which also proliferates the evanescent wave to achieve more information in terms of superresolution.

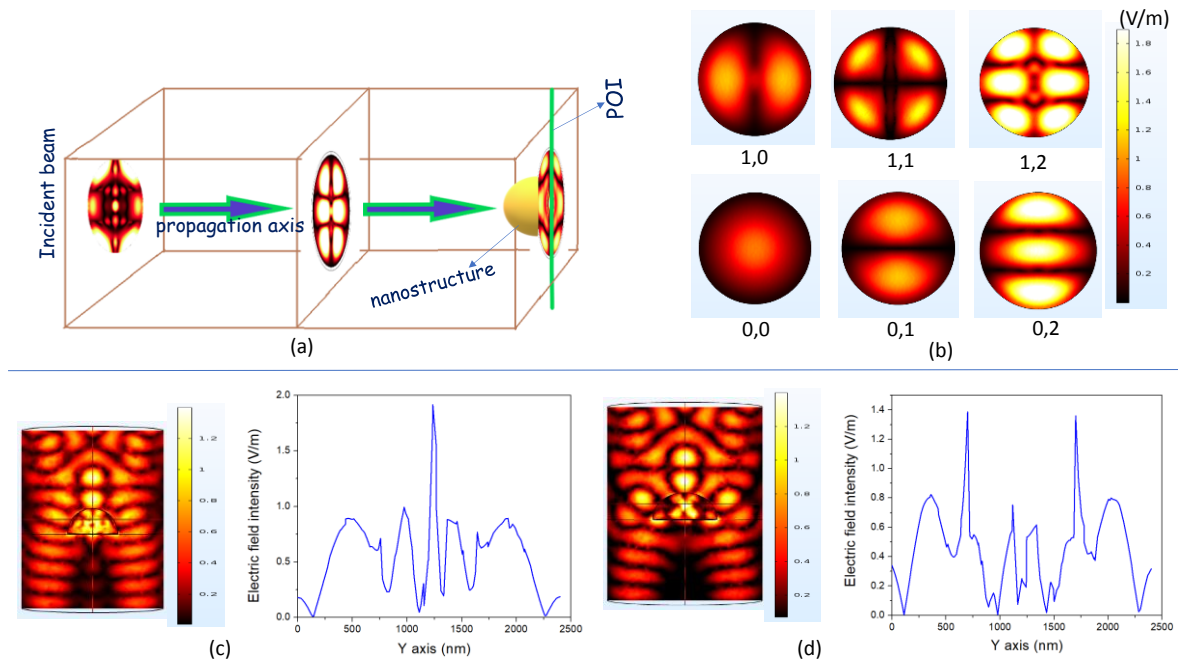


Fig 3: (a) Representation of our optical setup when a HG beam is launched on our nanorange e-SIL structure. The POI is mentioned where the near-field distribution is checked. (b) Different higher-order modes in a HG beam are shown here for our study. (A sharp peak is achieved in the near-field distribution) HG12 mode for our optimized structure. (d) Two distinct sharp peaks are observed for the same shape (e-SIL) with different parameters and under the HG10 beam.

Figure 3(c) confirms that HG beam (mode 12) incidence can produce a 65 nm ( $\sim\lambda/8.2$ ) superresolution image, as achieved by our high-index optimized e-SIL structure. This proves that the limit of resolution in the subwavelength region can result in better performance when we use structured beam illumination on a nanoscale lens structure instead of a plane Gaussian beam. Even the results obtained in the presence of the HG beam exhibit better performance than those obtained with LG beam incidence.

Nanoscale solid immersion lenses or microspheres are now capable of producing superresolution focal spots such as photonic nanojets only in the presence of high-index materials. Therefore, different refractive index materials have a strong effect on the superresolution spot at the POI.

We rigorously investigated and reported a comparative analysis of the FWHM values of the intensity distributions of near electric field spots

under plane Gaussian beam and Hermite Gaussian (HG) beam illumination after being focused by our optimized ellipsoid SIL nanostructure made from different materials (Figure 4). Even though a Gaussian beam provides a decent intensity profile in terms of the full width at half maximum (FWHM), a higher-order Gaussian beam profile (Hermite-Gaussian beam) still employs a predominant technique to attain better accuracy in terms of resolution efficiency, which can reach even below 70 nm. To justify the choice of solid immersion lens material for the proposed model, we compared the FWHM values of three different materials, i.e., diamond, GaN and the commonly available silica ( $\text{SiO}_2$ ) material. Figures 4 (a) to (f) show the electric field intensity distributions at the POI when both the plane Gaussian beam and the Hermite-Gauss beam are incident on our optimized nanostructure. In that case, we observed a very large difference in the resolution when we used diamond and GaN lens materials

compared with silica (Figure 4). Indeed, these high-index materials (diamond and GaN) result in low loss and a more confined beam profile, improving the overall system performance.

Finally, we obtain the highest resolution efficiency ( $\lambda/8.5$ ) under Hermite–Gauss beam illumination (incident wavelength = 532 nm) through diamond e-SIL on our optimized model (Figure 4 (f)). This explains why the Hermite–Gauss beam with a mode ( $HG_{12}$ ) provides the best resolution while detecting any sample at the plane of interest. Even we can improve the resolution efficiency in higher-order modes in the HG beam by further optimization. In the case of the  $HG_{10}$  mode, we obtained two distinct intensity peaks, which attained a resolution efficiency of  $\sim\lambda/7.4$  for the diamond lens material (Figure 3(d)). We set up a higher-order Gaussian beam with a beam waist of 750 nm to focus on our e-SIL geometry via a cylindrical aperture. When we apply the same higher-order mode ( $HG_{12}$ ) of the user-defined Hermite–Gaussian beam, the FWHM value reaches nearly 500 nm with a commonly available silica lens, which is not under the subdiffraction limit. Therefore, a lower index material makes the lens undesirable for use in nanoimaging in the subwavelength regime. Even diamond and GaN

lenses also produce FWHM values near  $\sim 210$  nm ( $\sim\lambda/2.5$ ) in terms of resolution when this structure is exposed to a plane Gaussian beam. Hermite–Gaussian (HG) beam illumination through the diamond e-SIL geometry is more relevant towards superresolution.

Even the same analogy as the LG beam was used here to ensure the robustness of our superresolution technique. We achieve a minimal deflection of the resolution efficiency from our optimal value. A higher beam waist of the incident beam helps to enhance the side lobes in the near-field distribution, which in turn decreases the resolution performance. We performed the overall study for only the high-index diamond lens structure. Figure 4(g) shows the impact of our structure on the resolution performance when the radius of the lens or semimajor axis of the lens is altered within a certain range. The shift in the resolution is almost minimal, and at higher radii, we obtain greater enhancement in the side lobes. Therefore, the resolution strength exhibits poor performance at the POI. This study could enhance the stability and practicality of the overall nanoimaging process while scanning any biological sample.

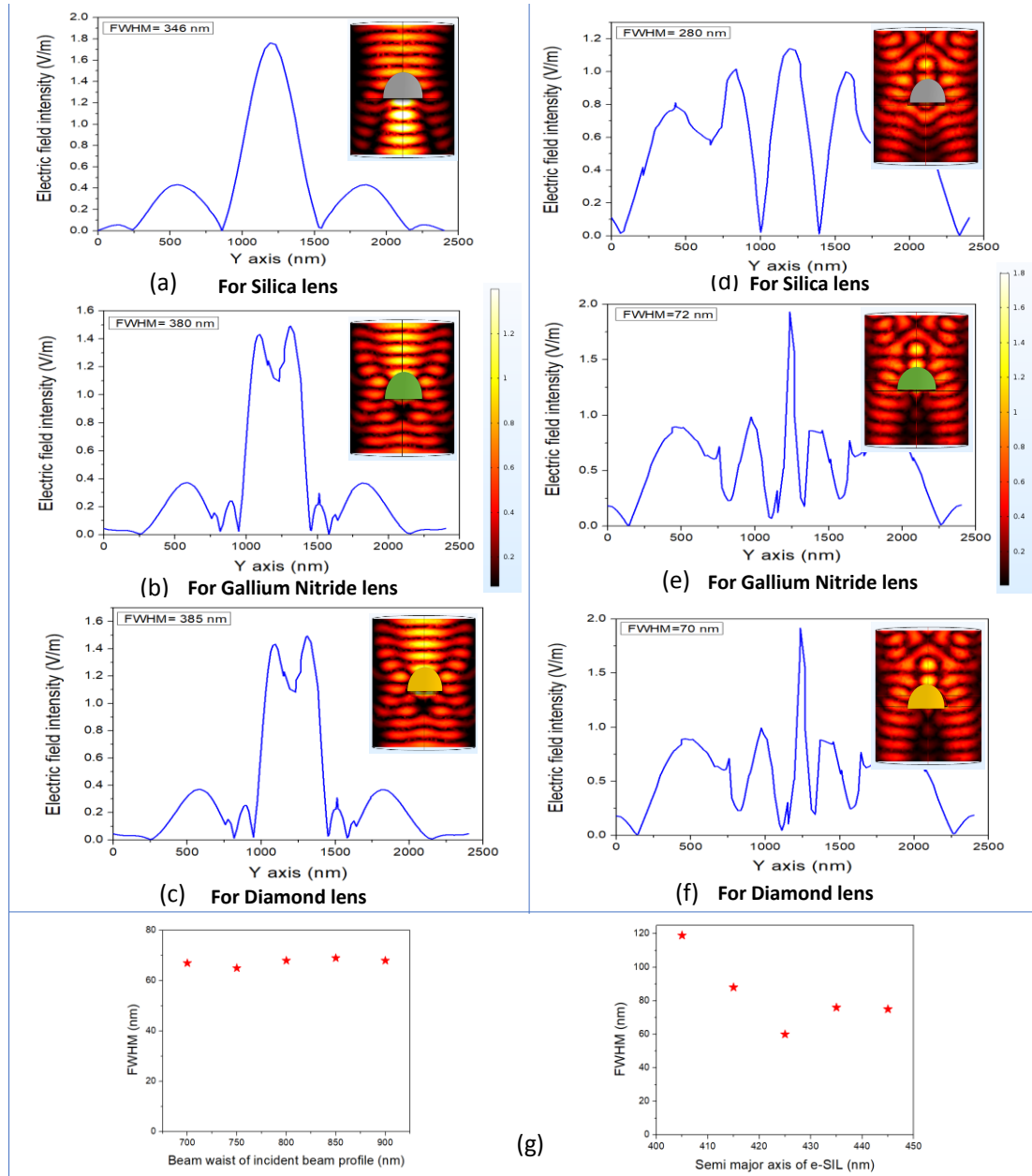


Fig. 4: (a)-(c) Plane Gaussian beam is launched on our nanorange e-SIL for three different lens materials (silica, GaN and diamond). (d)-(f) The same analysis is performed under HG beam illumination. We have shown the near electric field distribution, which is displayed in the inset. (g) This describes the impact of our structure on the resolution performance when the radius of the lens or semimajor axis of the lens is altered within a certain range.

#### Different structures under Laguerre- Gaussian and Hermite- Gaussian illumination:

After establishing superresolution in the subwavelength domain, we introduce different geometries to gain insight into the near-field resolution enhancement with the same vortex beam incidence. We introduced a high-index (diamond) material based different optical

structures under the illumination of two higher-order beams (Laguerre Gaussian beam and Hermite Gaussian beam), which is shown in Figure 5.

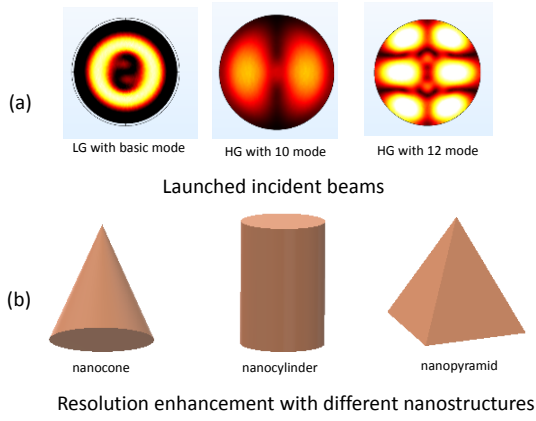


Fig. 5: Higher-order Gaussian beam illumination in the presence of different optical nanostructures. (a) We achieve our highest resolution performance in the presence of a basic LG beam and an HG beam for two modes. The beam shape is displayed in the figure. (b) Different structures, such as nanocones, nanocylinders and nanopyramids, are used to achieve superresolution. This could be an evidence that improving the superresolution technique with different geometries could modify the beam profile characteristics.

**Geometrical analysis with Laguerre -Gaussian beam illumination:**

Here we discuss how we launched a Laguerre-Gaussian beam from an aperture of NA=0.6 and coupled it with three nanostructures of different shapes. Later, we implemented the same analogy in this study and measured the near electric field intensity at the POI. Figure 6(a) depicts the coupling of the LG beam with the diamond-based cone structure, which generates photonic nanojets at the POI. The optimized dimension of the diamond cone structure is considered as follows: the bottom radius is 430 nm, and the height is 730 nm. It is expected that a higher resolution with a lower FWHM value can be obtained with this geometry modification. For example, the geometry of the nanocone structure generates a sharp electric field intensity distribution at the POI, which results in higher resolution under 532 nm beam incidence. Figure 6(a) shows the electric field distribution when a Laguerre Gaussian beam is incident on the diamond cone structure. We placed our optical structure at the focal plane of the incident beam. Even shifting the focal point along the z-axis significantly affects near-field spot

generation, but in this study, we do not move the focal point frequently for a single geometry once after it is set. This design provides an increase in the resolution in the presence of an LG beam, which is investigated here. We present an optimized near electric field intensity pattern at the POI for this cone structure, which is shown in the inset (Figure 6(a)). This figure also shows that we achieved an FWHM of 57 nm ( $\sim\lambda/9.5$ ) with the LG beam incident on the cone at its optimum value. Compared with the earlier design, the subwavelength optical structure can achieve resolution in the superresolution regime, which is improved. In addition to improving the resolution, the cone structure also has several advantages, such as reducing the side lobe intensity, enhancing the contrast of the field distribution, and obviously shifting the focus near the POI.

We performed a geometrical sweep (the bottom radius of the cone structure was varied within  $\pm 30$  nm) of the proposed cone structure for three different beams. Here, the resolution stability drastically decreases with a wide variation in the cone radius, especially for the LG beam.

Next, the tolerance limit of the resolution efficiency is studied with a variation in the cone radius and different beam waists to make the simulation results more feasible for three different incident beams. Figure 6(b) shows a stable near-field intensity profile at the POI with wide beam waist variation. Moreover, for the LG beam, the dependence on the beam waist has a negligible effect on the resolution efficiency. This design offers excellent stability for the FWHM value even with a large beam waist variation (Figure 6(c)).

From a stability point of view, dark field application is beneficial, and in the case of superresolution formation, the application of an LG beam is preferable for resolution enhancement because it provides the spatial distribution of the incoming incident beam. The shape of the geometry is a crucial building block of such resolution control. The perfect optimization helps to achieve a more convergent beam at the plane of interest, which works well under LG beam illumination.

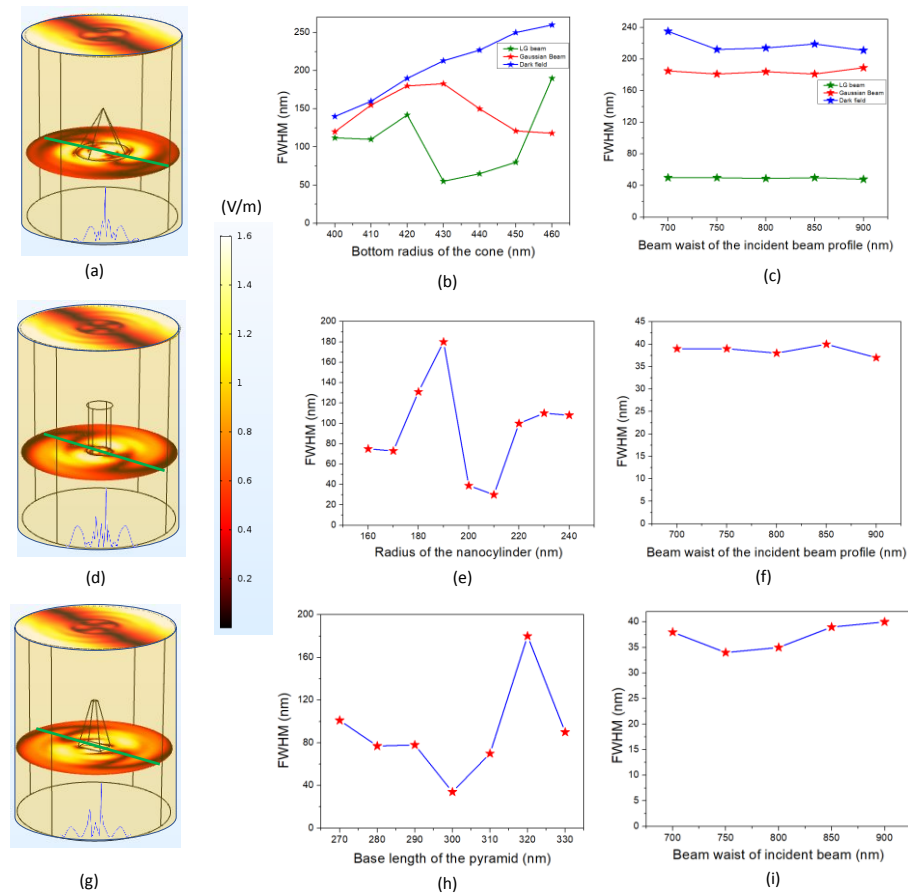


Fig. 6: (a) LG beam is launched on a nanorod cone structure. (b) (c) Geometrical tolerances of the bottom radius and resolution variation for different beam waists are displayed here for the same structure. We compared the same study in the presence of a plane Gaussian beam and dark field illumination for the same cone structure. (d)(e)(f) The near electric field distribution at POI is shown here for the nanocylinder structure. The optimized intensity pattern is shown in the inset. The changes in the FWHM with respect to the radius of the cylinder and the variation in the beam waist are shown. (g) (h) (i) A detailed investigation of the electric field distribution at the POI is displayed (when a nanoscale pyramid structure is present). The effects of the geometry of the pyramid and the beam waist of the incident beam on the resolution measurement are studied.

Geometry-dependent resolution control in the subwavelength domain is an important factor in this work; therefore, we introduce several simple and unique designs that can be utilized as nanolenses to converge the beam to achieve a tiny focal spot. In the case of nanocylinder, as shown in Figure 6(d), to improve the resolution efficiency in the superresolution regime. Here, we consider a basic-order LG beam to launch from the circular aperture with the same NA, which is coupled with a high-index (r.i.=2.425) material. The near-field

distribution indicates that we attain a super resolution even below 50 nm, which is much better than the earlier findings. We achieved this result with an optimized radius of 200 nm and a height of 725 nm for our proposed nanocylinder. The best resolution observed for this optimized cylinder is 39 nm in terms of the FWHM value, which is equivalent to  $(\lambda/13.5)$ . The LG beam creates a smaller side lobe in its near-field distribution, which is feasible in this case. Two important factors (i.e., radius and the beam waist)

were investigated to confirm our structural tolerance. We varied the radius of the nanocylinder within a range of 30 nm from our optimized model. However, from Figure 6(e), we observe that the tolerance slightly fluctuates when the radius is below the optimized parameter. In the case of the beam waist, we noticed stable variation in the FWHM measurement, which shows better performance (resolution  $\sim \lambda/14$ ) even after increasing the beam waist up to 900 nm (Figure 6(f)).

Finally, we tested a pyramid structure in the nanoscale range, which produces a best FWHM value for the near electric field distribution at the POI of our predicted model. We obtain an FWHM value of 34 nm, which is equivalent to the ( $\lambda/15.5$ ) resolution efficiency (Figure 6(g)). This optical nanostructure with LG beam coupling works well under this regime, which supports a significant improvement in the domain of superresolution

imaging. This offers a tight focal spot with lower-intensity side lobes, which enhances the resolution efficiency at the POI. The geometrical tolerances of various base lengths of the nanoscale pyramid structure and the incident beam waist are investigated. We have achieved significant stability over a wide range of beam waists. Figure 6(h) shows that we achieve better stability in the superresolution regime, which is much better than the other two structures under LG beam illumination. Near lower base lengths, two highly intense distinct peaks are observed, and fewer scattered beams are attained at the POI. This enhances the resolution efficiency in terms of the FWHM values. The performance stability slightly deviates when the base length of the pyramid is increased. In the next diagram (Figure 6(i)), we studied the tolerance of the beam waist of the incident LG beam. The best resolution is attained at the optimized parameter, which is the best achieved result in this structure beam illumination.

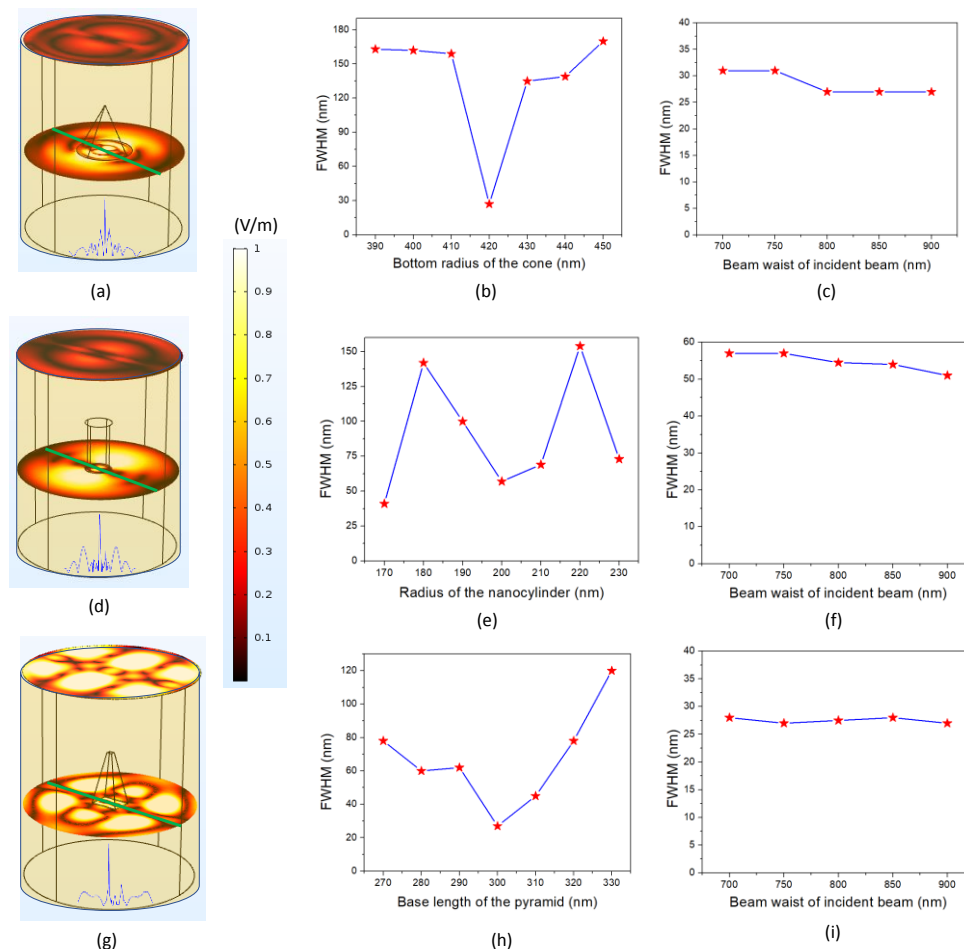


Fig. 7: (a) The HG10 beam is launched on a nanorod cone structure. (b) (c) Geometrical tolerances of the bottom radius and resolution variation for different beam waists are displayed here for the same structure.

(d)(e)(f) The near electric field distribution at POI is shown here for the nanocylinder structure. The optimized intensity pattern is shown in the inset. The changes in the FWHM with respect to the radius of the cylinder and the variation in the beam waist are shown. (g) (h) (i) A detailed investigation of the electric field distribution at the POI is displayed (when a nanoscale pyramid structure is present). The effect on resolution measurement with respect to geometry of the pyramid and the beam waist of the incident beam is studied.

### ***Geometrical analysis with Hermite Gaussian beam illumination:***

Here, we launched a Hermite- Gaussian beam to all three different optical structures, and we achieved a superresolution of up to 27 nm in terms of FWHM values, which is equivalent to  $(\lambda/19.5)$ . Figures 7(a), (d), and (g) present the incident beam mode at the aperture with an NA=0.6 and the near-field distribution at the POI of three different optical structures, which can provide resolution measurements implicitly. We obtain our best result with this diamond-based cone-shaped optical structure in the presence of a Hermite Gauss beam with the HG 10 mode. Here, the presence of a side lobe in the near-field distribution is almost negligible for our optimized parameter. Rather, from a stability point of view, if we change the bottom radius of the cone, our electric field distribution shows instability in the resolution performance. Our FWHM value shifted above the superresolution regime, which proves that our system is highly stable only at the optimized parameter. Coupling between the HG 10 mode incident beam and the cylindrical diamond-based optical nanostructure is shown in Figure 7(d). Here, we cannot achieve resolution efficiency, unlike other structures, but indeed, it also has an FWHM value of 57 nm  $(\lambda/9.3)$ . In this case, the radius of the nanocylinder exhibits more deflection when it deviates from the optimized parameter. Rather, our optical structure displays significant improvement when we move toward the larger beam waist of the incident beam. The near-field distribution shows a slightly higher side lobe with lower intensity and not much dominance, which does not greatly affect our sharp peak at the optimized parameter. Finally, we maintained our nanoscale pyramid structure under HG12 mode beam illumination through the same NA=0.6 aperture. This structure can generate a tiny focal spot at the POI with a smaller side lobe field distribution. We obtain a resolution of  $(\lambda/19.5)$  with the optimized parameter, which is

more stable when we test the geometrical tolerance of the structure. When the base length of the pyramid is below its optimized value, it provides better efficiency under the superresolution regime. However, near the higher base length of the pyramid, there is a slight increase in the FWHM value, which is far from the superresolution limit. In the case of beam waist variation, it provides better stability than the other three structures.

### **CONCLUSIONS:**

In summary, we performed a numerical analysis for different geometries (e-SIL, cone, cylinder and pyramid) under different types of incident beams, i.e., Gaussian, dark field, Laguerre- Gaussian and Hermite- Gaussian beam illuminations. The near electric field intensity pattern at the plane of interest (bottom surface of the designs) is computationally investigated and analyzed. We also compared the FWHM values for different beam waists and finally obtained values of 34 nm and 27 nm under LG and HG beam illuminations for our optimized nanostructures, which provides a superresolution over the diffraction limit. The proposed techniques can be utilized to cover a wide range of applications, ranging from the scanning of objects to the nanorange lithography technique, with the help of this sharp narrow intensity profile. In addition, we can even incorporate this technique to many other superresolution techniques in the field of nanophotonics applications.

### **References:**

1. E. Abbe, Arch. Mikrosk. Anat. 9, 413 (1873).
2. H. Heinzelmann, D. W. Pohl, Scanning near-field optical microscopy, Appl. Phys. A 59 (1994) 89-101.
3. P. Bharadwaj, B. Deutsch, L. Novotny, Optical antennas, Adv. Opt. Photonics, 1 (2009) 438-483

4. Pendry, J. B. Negative refraction makes a perfect lens. *Phys. Rev. Lett.* 85, 3966 – 3969 (2000).
5. Fang, N., Lee, H., Sun, C. & Zhang, X. Subdiffraction-limited optical imaging with a silver superlens. *Science* 308, 534 – 537 (2005).
6. Taubner, T., Korobkin, D., Urzhumov, Y., Shvets, G. & Hillenbrand, R. Near-field microscopy through a SiC superlens. *Science* 313, 1595 (2006).
7. Huang, X. H., Jain, P. K., El-Sayed, I. H. & El-Sayed, M. A. Plasmonic photothermal therapy (PPTT) using gold nanoparticles. *Lasers Med. Sci.* 23, 217 – 228 (2008).
8. J. Rho, Z. Ye, Y. Xiong, X. Yin, Z. Liu, H. Choi, G. Bartal, and X. Zhang, *Nat. Commun.* 1, 143 (2010).
9. Mason, D. R., Jouravlev, M. V. & Kim, K. S. Enhanced resolution beyond the Abbe diffraction limit with wavelength-scale solid immersion lenses. *Opt. Lett.* 35, 2007 – 2009 (2010).
10. Lee, J. Y. et al. Near-field focusing and magnification through self-assembled nanoscale spherical lenses. *Nature* 460, 498 – 501 (2009).
11. L. Novotny, D. W. Pohl, and B. Hecht, "Scanning near-field optical probe with ultrasmall spot size," *Opt. Lett.* 20(9), 970–972 (1995).
12. E. T. F. Rogers, J. Lindberg, T. Roy, S. Savo, J. E. Chad, M. R. Dennis, and N. I. Zheludev, "A superoscillatory lens optical microscope for subwavelength imaging," *Nat. Mater.* 11(5), 432–435 (2012).
13. M. S. Kim, T. Scharf, M. T. Haq, W. Nakagawa, and H. P. Herzig, *Opt. Lett.* 36, 3930 (2011).
14. Clarke, Daniel DA, and Ortwin Hess. "Near-field strong coupling and entanglement of quantum emitters for room-temperature quantum technologies." *Photonix* 5(1) 33, (2024).
15. Zhang, Xiaoqiuyan, Min Hu, Xiang Zhao, Jie Zhou, Zhuocheng Zhang, Jun Zhou, Weiling Fu, and Shenggang Liu. "Biomedical applications of terahertz near-field imaging." In 2021 46th International Conference on Infrared, Millimeter and Terahertz Waves (IRMMW-THz), 1-2. IEEE, 2021.